ELSEVIER

Contents lists available at ScienceDirect

# Journal of Magnetism and Magnetic Materials

journal homepage: www.elsevier.com/locate/jmmm





# Magnetization distribution in $Cu_{0.6}Mn_{2.4}Ge_2$ ferromagnet from polarized and non-polarized neutron powder diffraction aided by density-functional theory calculations

Zachary P. Tener<sup>a</sup>, Vincent Yannello<sup>b</sup>, Jenifer Willis<sup>a</sup>, V. Ovidiu Garlea<sup>c,\*</sup>, Michael Shatruk<sup>a,d,\*</sup>

- <sup>a</sup> Department of Chemistry and Biochemistry, Florida State University, Tallahassee, FL 32306, United States
- <sup>b</sup> Department of Chemistry, Biochemistry and Physics, University of Tampa, Tampa, FL 33606, United States
- <sup>c</sup> Neutron Scattering Division, Oak Ridge National Laboratory, Oak Ridge, TN 37831, United States
- <sup>d</sup> National High Magnetic Field Laboratory, Tallahassee, FL 32310, United States

# ARTICLE INFO

Keywords: Ferromagnetism Magnetic structure Neutron scattering Magnetocaloric effect

# ABSTRACT

The crystal structure and magnetic properties of  $Cu_{0.6}Mn_{2.4}Ge_2$  have been re-investigated by a combination of extensive magnetic measurements and neutron scattering experiments, aided by electronic structure calculations. The material is found to be a soft ferromagnet with the ordering temperature  $T_{\rm C}=316$  K. The magnetocaloric effect evaluated from field-dependent magnetization isotherms is equal to 1.2 J/(kg·K) and 2.5 J/(kg·K) under the maximum applied magnetic field of 2 T and 5 T, respectively. The compound crystallizes in the hexagonal space group  $P6_3/mmc$ . A complex structural disorder necessitated testing of several disorder models against the results of non-polarized and polarized neutron scattering experiments and magnetization measurements. Simulations at the density-functional theory level were also performed to identify the most robust solution that properly described the data observed. The final magnetic structure model reveals non-equal magnetic moments on the Mn1 and Mn2 atoms (2.29(9)  $\mu_{\rm B}$  and 2.7(1)  $\mu_{\rm B}$ , respectively) and the presence of vacancies and minor Cu substitution defects in both Mn sites. The work demonstrates how the non-polarized and polarized neutron scattering methods can be combined with electronic structure calculations to establish the microscopic structure of magnetic materials with complex crystallographic disorder.

# 1. Introduction

Recently, Shanavas and Singh [1] reported a theoretical study of  $CuFe_2Ge_2$ , prompted by the observation of superconductivity in  $YFe_2Ge_2$  [2–4]. They demonstrated that the electronic structure of  $CuFe_2Ge_2$  should be conducive to itinerant (band) ferromagnetism, which was subsequently confirmed experimentally [5]. Both the theoretical and experimental studies revealed competing ferromagnetic (FM) and antiferromagnetic (AFM) interactions between the Fe sites in  $CuFe_2Ge_2$ . This competition results in the suppression of the AFM state even in relatively weak applied magnetic fields in favor of the FM state. It was also suggested that electron doping, e.g., by substitution of Co for Fe, should shift the Fermi level to a pseudo-gap in the electronic density of states (DOS) and potentially induce superconductivity – a hypothesis that still awaits its verification. Upon examination of the DOS plot for  $CuFe_2Ge_2$ ,

we have become interested in an opposite effect: lowering the electron count in this system should position the Fermi level more robustly within the high DOS peak, which appears below the pseudo-gap, and strengthen the itinerant FM behavior. Indeed, the material with the lower electron count, "CuMn<sub>2</sub>Ge<sub>2</sub>", was reported in 1965 and shown to undergo FM ordering at  $T_{\rm C}=339~{\rm K}$  [6]. Later, it was demonstrated that this compound was more accurately described as  ${\rm Cu}_{0.6}{\rm Mn}_{2.4}{\rm Ge}_2$  [7]. It exhibits a superstructure derived from the hexagonal  $\gamma\text{-Ni}_3{\rm Sn}_2$  structure type [8] that, in turn, is a defect variant of the Ni<sub>2</sub>In structure type [9]. The orthorhombic structure of  ${\rm CuFe}_2{\rm Ge}_2$  is also derived from the Ni<sub>2</sub>In structure type, as was discussed by Zavalij et al. [10]. Up to date, no further studies of  ${\rm Cu}_{0.6}{\rm Mn}_{2.4}{\rm Ge}_2$  have been described, although its FM phase transition is appealing for investigating both magnetic and magnetocaloric properties.

Herein, we report a detailed investigation of magnetic and structural

<sup>\*</sup> Corresponding authors at: Neutron Scattering Division, Oak Ridge National Laboratory, Oak Ridge, TN 37831, United States (V.O. Garlea); Department of Chemistry and Biochemistry, Florida State University, Tallahassee, FL 32306, United States (M. Shatruk).

E-mail addresses: garleao@ornl.gov (V. Ovidiu Garlea), mshatruk@fsu.edu (M. Shatruk).

properties of  $Cu_{0.6}Mn_{2.4}Ge_2$  and establish its crystal and magnetic structures from neutron scattering data. We demonstrate that the model proposed by Zavalij *et al.* [7] does not properly describe experimentally observed neutron scattering. We also find that two crystallographically unique Mn sites exhibit different magnetic moments in the FM ordered state, and we provide a theoretical analysis that justifies the observed difference. Based on these studies, a new model of the crystal structure of  $Cu_{0.6}Mn_{2.4}Ge_2$  is proposed, which agrees with the observed magnetic and neutron scattering data and with the conclusions of the theoretical analysis.

# 2. Materials and methods

# 2.1. Synthesis

All manipulations during sample preparation were carried out in an argon-filled dry box (content of  $\rm O_2 < 0.1$  ppm). All starting materials were obtained from Alfa Aesar. Powders of manganese (99.95% metals basis) and germanium (99.999%) were used as received while the copper powder was additionally purified by heating in a flow of  $\rm H_2$  gas for 5 h at 475 K. Fused silica tubes were obtained from National Scientific Corporation, Inc. (Quakertown, PA). The synthetic procedure followed the previously reported synthesis of  $\rm Cu_{0.6}Mn_{2.4}Ge_2$  [7]. A pelletized stoichiometric mixture of the elements was arc-melted, and the ingot obtained was sealed under vacuum ( $\rm <10^{-4}$  mbar) in a 10 mm inner diameter fused silica tube. The ingot was annealed at 873 K for 10 days, after which the furnace was opened and the sample was quickly quenched into ice water. The quenching step was crucial to avoid decomposition of the target phase into related binary compounds.

# 2.2. Powder X-ray diffraction

Powder X-ray Diffraction (PXRD) was carried out on a Panalytical X'Pert Pro diffractometer equipped with a graphite monochromator, an X'Celerator detector, and a Cu-K $\alpha$  radiation source ( $\lambda=1.54187$  Å). The data were collected in the  $2\theta$  range of  $10-80^\circ$  with a step of  $0.017^\circ$  and a total collection time of 6 h. The PXRD patterns were analyzed with the HighScore Plus software [11].

# 2.3. Neutron scattering

Neutron scattering measurements were performed at the Oak Ridge National Laboratory (ORNL). Neutron powder diffraction (NPD) data were collected at 375, 300, and 100 K, using the HB-2A high-resolution diffractometer at the ORNL High-Flux Isotope Reactor facility [12]. A sample of  $\sim 3$  g held in a cylindrical vanadium container was placed in a top-loading Janis closed-cycle refrigerator system. The  $\lambda=1.539$  Å radiation was provided by a vertically focused Ge (115) monochromator. The data were collected by scanning the detector array consisting of 44  $^3$ He tubes, to cover the total 20 range of 7°–133° in steps of 0.05°. Overlapping detectors for a given step served to average the counting efficiency of each detector. Rietveld refinement of the collected data was carried out using FullProf [13]. An analysis of symmetry-allowed magnetic models was performed using SARAh representational analysis software [14].

The non-polarized NPD experiments performed at HB-2A were complemented by polarized neutron scattering measurements using the HYSPEC spectrometer at the ORNL Spallation Neutron Source [15]. The sample was prepared as a compacted pellet and loaded inside a permanent-magnet yoke that provided a vertical magnetic field of 0.4 T at the sample position. This assembly was then loaded in a bottom-loading closed-cycle refrigerator. The monochromatic polarized neutron beam with the wavelength  $\lambda=2.02$  Å was obtained by reflection from a Heusler monochromator, and a Mezei flipper was used to flip the spin direction of the incident neutron beam. The effective polarization factor of the incident neutron beam was estimated to be about

86%, using the scattering from a Heusler single-crystal probe. The data were collected using  $^3$ He linear position-sensitive tube detectors assembled into 20 sets of 8-packs that covered an angular range of  $60^\circ$  in the horizontal scattering plane and a vertical acceptance of  $15^\circ$ . Flipping difference profiles were obtained from successive measurements with polarized beam oriented parallel and anti-parallel to the external magnetic field. No polarization analysis of the scattered beam is performed using this method [16].

# 2.4. Physical measurements

The elemental analysis was performed on an FEI Nova 400 Nano scanning electron microscope equipped with an energy dispersive X-ray (EDX) spectrometer. Multiple locations on a pelletized polycrystalline sample were probed to establish the statistically averaged composition of each sample. Magnetic measurements were performed with a magnetic property measurement system (MPMS-XL, Quantum Design) equipped with a superconducting quantum interference device (SQUID). Direct current (DC) magnetic susceptibility measurements were carried out in the zero-field-cooled (ZFC) and field-cooled (FC) modes in the 1.8–300 K temperature range, with an applied field of 10 mT. Field-dependent magnetization measurements were performed at 2, 100, and 250 K in the applied magnetic field that varied from 0 to 7 T.

# 2.5. Quantum-chemical calculations

The density-functional theory (DFT) electronic structure calculations were performed using the Spin-Polarized Relativistic Korringa-Kohn-Rostoker (SPR-KKR) package [17]. The nuclear structural parameters (unit cell dimensions, occupancy ratios, and atomic coordinates) for  $\text{Cu}_{0.6}\text{Mn}_{2.4}\text{Ge}_2$  were taken both from the reported room-temperature crystal structure [7] and from the refined structural model obtained from the neutron powder diffraction. The default settings generated were used for the electronic structure optimization. A mesh of 4000 k-points was used for all calculations. Spin-polarized calculations were performed by initializing the number of unpaired electrons to be equal to 7 for each Mn atom and to zero for all other atoms. Modifying this initial magnetization value to experimentally observed moments had no effect on the final value of the calculated magnetic moment per Mn site.

# 3. Results and discussion

# 3.1. Synthesis and structure

 $\text{Cu}_{0.6}\text{Mn}_{2.4}\text{Ge}_2$  was synthesized by arc-melting followed by homogenizing annealing at 600 °C, using the stoichiometry reported by Zavalij et al. [7]. Rapid quenching of the annealed product was crucial to avoid decomposition of the target phase into binary germanides. The PXRD analysis confirmed a nearly phase-pure sample. The Cu:Mn:Ge ratio established from the EDX analysis was 0.56(2):2.36(6):2.00(5), in good agreement with the nominal composition. Therefore, we will use the formula  $\text{Cu}_{0.6}\text{Mn}_{2.4}\text{Ge}_2$  in the following discussion. It should be noted that using ratios of elements deviating from the nominal composition led to higher amount of impurities, such as  $\text{Cu}_3\text{Ge}$  and  $\text{Mn}_{11}\text{Ge}_8$ , observed in the PXRD pattern.

Since the crystal structure of  $Cu_{0.6}Mn_{2.4}Ge_2$  was previously reported only briefly [7], we discuss it in greater detail, based on the Rietveld refinement of the NPD data collected at 375 K (see Table 2 in the Neutron Diffraction section). The compound crystallizes in the  $P6_3/mmc$  space group, with five crystallographically distinct atomic sites. The Mn1 (6g) and Mn2 (6h) sites are surrounded by Ge atoms, resulting in MnGe<sub>6</sub> octahedra and MnGe<sub>5</sub> trigonal bipyramids, respectively. The Mn–Ge distances are in the range of 2.532–2.694 Å for the MnGe<sub>6</sub> octahedra and 2.497–2.646 Å for the MnGe<sub>5</sub> bipyramids, while the Mn–Mn distances range from 2.584 to 2.755 Å. The Mn-Ge distances are comparable to those observed in binary manganese germanides, e.g.,

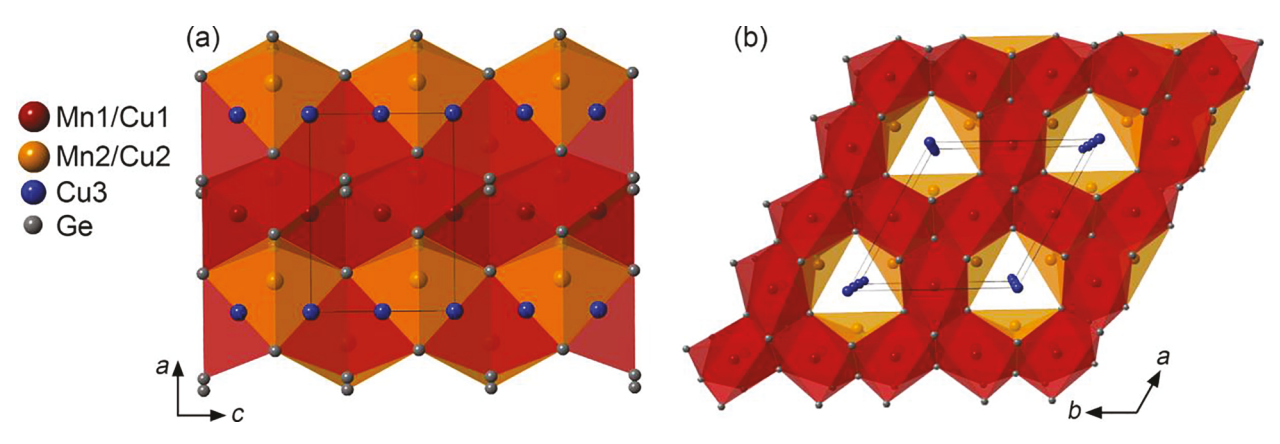


Fig. 1. The crystal structure of  $Cu_{0.6}Mn_{2.4}Ge_2$ : (a) a view down the *b* axis, showing the alternating layers of MnGe<sub>6</sub> octahedra (red) and MnGe<sub>5</sub> trigonal bipyramids (orange); (b) a view down the *c* axis, showing the channels filled with rows of Cu atoms.

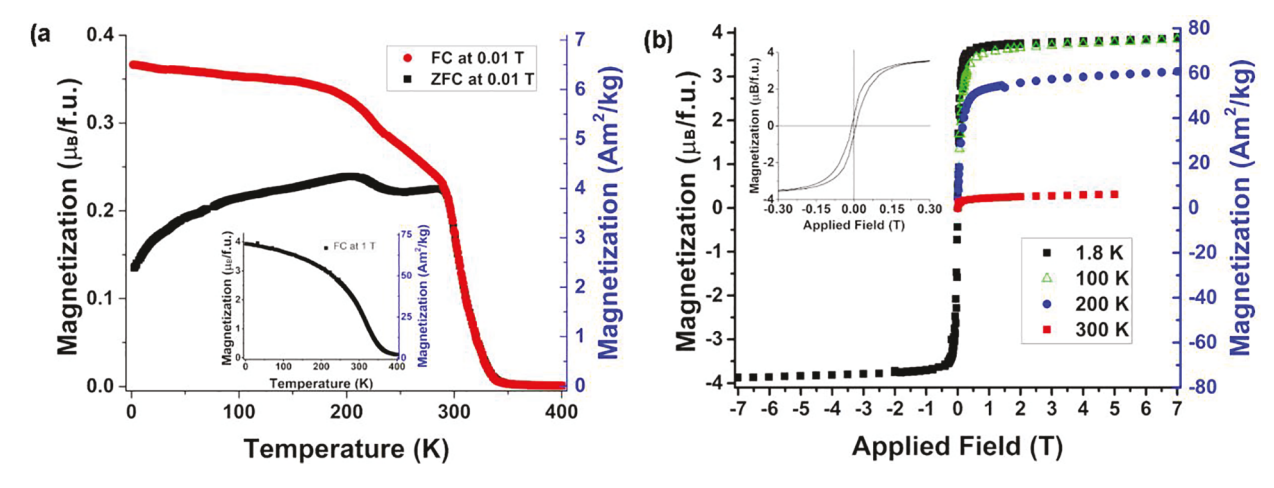
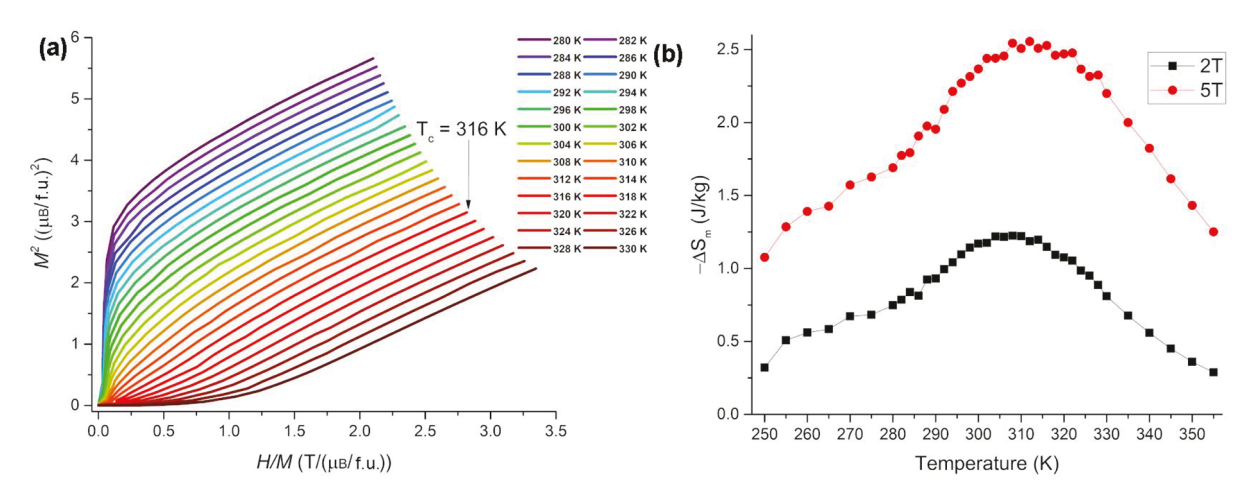


Fig. 2. (a) The temperature-dependent magnetization of  $Cu_{0.6}Mn_{2.4}Ge_2$  in the applied magnetic field of 0.01 T and 1 T (inset). (b) Field-dependent magnetization isotherms measured at different temperatures, with a very small hysteresis seen in the 1.8 K data (inset).

2.408–2.746 Å for  $Mn_2Ge$  [18] and 2.579–2.668 Å for  $Mn_3Ge$  [19]. The layers of octahedra and trigonal bipyramids run parallel to the ab plane and alternate along the c axis (Fig. 1a). Within this framework, channels filled with Cu3 (2a) atoms are observed parallel to the c axis, with the Cu–Cu distance of 2.566 Å (Fig. 1b). The full occupancy of all unique sites should lead to a composition  $Cu_{0.5}Mn_3Ge_2$ . The experimentally verified composition,  $Cu_{0.6}Mn_{2.4}Ge_2$ , is achieved by allowing mixed Mn/Cu occupancy of the Mn1 and Mn2 sites, as well as presence of

vacancies in these sites. The model proposed by Zavalij *et al.* from the analysis of PXRD data [7] suggested that the Mn1 site was completely occupied by Mn atoms while the Mn2 site contained 60% of Mn atoms, 6.7% of Cu atoms, and 33.3% of vacancies.  $\text{Cu}_{0.6}\text{Mn}_{2.4}\text{Ge}_2$  is thus isostructural with  $\text{Fe}_{13}\text{Ge}_8$  ( $\equiv \text{Fe}_{3.25}\text{Ge}_2$ ), which is derived from the parent structure of  $\text{Ni}_2\text{In}$  by doubling the *a* axis and creating 17% of vacancies in the Fe(6h) site [20]. Nevertheless, our crystal structure and magnetic moment analysis suggests that the defect distribution in the 6g and 6h



 $\textbf{Fig. 3.} \ \ \text{The Arrott plot (a) and temperature-dependent entropy changes (b) for } \ \text{Cu}_{0.6} \text{Mn}_{2.4} \text{Ge}_2.$ 

sites is more complex, as will be discussed in the later sections.

# 3.2. Magnetic properties

Measurements performed under applied magnetic field of 10 mT revealed an abrupt increase in both FC and ZFC magnetization at  $\sim 340$ K, followed by an additional and weaker transition at  $\sim 225$  K, below which the magnetization saturates (Fig. 2a). Such behavior suggests an occurrence of FM ordering in Cu<sub>0.6</sub>Mn<sub>2.4</sub>Ge<sub>2</sub>, in agreement with the earlier work that reported FM transition at  $T_{\rm C}=339~{\rm K}$  based on the Curie-Weiss fit of inverse susceptibility data in the paramagnetic regime [6]. To determine the FM ordering temperature more accurately, we constructed an Arrott plot, which gave a value of  $T_{\rm C} = 316$  K (Fig. 3a). (It will be shown below that this value is also in a better agreement with magnetocaloric properties of Cu<sub>0.6</sub>Mn<sub>2.4</sub>Ge<sub>2.</sub>) Additionally, a Curie-Weiss fit  $[1/\chi = (T - \theta)/C]$  performed in the range from 374 to 400 K (Fig. S1) resulted in a Weiss constant of  $\theta = 319.5(2)$  K and a Curie constant of C = 4.56(1) emu·K/mol per formula unit (f.u. =  $Cu_{0.6}Mn_{2.4}Ge_2$ ), which gives an effective magnetic moment  $\mu_{eff}=3.90$ (4)  $\mu_B$  per Mn atom. This value slightly exceeds the effective moments per Mn atom reported for  $Mn_{11}Ge_8$  (3.26  $\mu_B$ ) [21],  $Mn_5Ge_3$  (3.50  $\mu_B$ ) [22], and MnGe (3.68  $\mu_B$ ) [23].

Notably, when the applied field was increased to 1 T, the FM transition became more gradual but the weaker transition observed at  $\sim$  225 K was suppressed (Fig. 2a and inset). Thus, we attribute the second transition to the presence of  $Mn_{11}Ge_8$  impurity phase observed in a small amount along with non-magnetic  $Cu_3Ge$  in non-polarized neutron diffraction patterns.  $Mn_{11}Ge_8$  has a complex magnetic phase diagram [21] that includes an FM transition at  $\sim\!274$  K. Thus, the weak second transition observed in our sample, most likely, is a tail of the FM ordering from the minor  $Mn_{11}Ge_8$  impurity. It is unlikely that this anomaly is due to the presence of any other known Mn-Ge binary material, since the observed temperature range is inconsistent with magnetic behavior reported for such binary phases [24].

The isothermal field dependence of magnetization measured at 300, 200, 100, and 1.8 K clearly confirms the FM behavior of  ${\rm Cu_{0.6}Mn_{2.4}Ge_2}$  (Fig. 2b). The maximum magnetization gradually increases as the temperature is lowered, reaching the full saturation at 100 K and 1.8 K. At the lowest temperature, the material behaves as a soft ferromagnet with the coercive field  $H_{\rm c}=8.3$  mT and saturation magnetization  $M_{\rm sat}=3.85$   $\mu_{\rm B}$  per f.u.

Due to the FM ordering near room temperature and the low coercivity value, we examined  $\text{Cu}_{0.6}\text{Mn}_{2.4}\text{Ge}_2$  as a potential magnetocaloric material. The magnetic entropy change  $(-\Delta S_{\text{m}})$  and relative cooling power (RCP) for a ferromagnet in an applied field were calculated from the field-dependent isotherms collected in the range from 250 to 360 K with a temperature increment  $(\Delta T)$  of 2 or 5 K, depending on the proximity of temperature to  $T_{\text{C}}$  (Fig. S2). The  $-\Delta S_{\text{m}}$  values were found by approximating the integral Maxwell equation with a sum [25]:

$$\Delta S_m(T,\Delta H) = \sum_{0}^{H_{\max}} \frac{M_i - M_{i-1}}{T_i - T_{i-1}} \Delta H$$

where  $M_i$  and  $M_{i-1}$  are the magnetization values observed for adjacent isotherms measured at  $T_i$  and  $T_{i-1}$ , respectively,  $T_i - T_{i-1} = \Delta T$ , and  $\Delta H$  is the step in the magnetic field, varied from 0 to  $H_{\text{max}}$ . The maximum entropy change is observed around 310 K (Fig. 3b), with  $-\Delta S_{\text{m}} = 1.2 \text{ J/(kg·K)}$  and 2.5 J/(kg·K) at  $H_{\text{max}} = 2 \text{ T}$  and 5 T, respectively. The RCP can be estimated as the product of these maximum values by the full-width at half-maximum (FWHM) of the  $-\Delta S_{\text{m}}$  peak (Fig. 3b), which yields the RCP values of 63 J/(kg·K) and 143 J/(kg·K) at 2 and 5 T, respectively. Note that the temperature at which the  $-\Delta S_{\text{m}}$  maximum is observed agrees better with the  $T_{\text{C}}$  value of 316 K determined from the Arrott plot, as compared to the value of 339 K reported earlier [6].

The maximum values of  $-\Delta S_m$  and RCP observed for  $\text{Cu}_{0.6}\text{Mn}_{2.4}\text{Ge}_2$  are substantially lower than those reported for benchmark Mn-

Table 1 The values of  $-\Delta S_m$  and RCP observed for  $\text{Cu}_{0.6}\text{Mn}_{2.4}\text{Ge}_2$  in comparison to the characteristics of related manganese germanides and benchmark magnetocaloric materials.

Material	$-\Delta S_{\rm m}$ at 2 T/5 T, J/(kg·K)	RCP at 2 T/5 T, J/(kg·K)
Cu <sub>0.6</sub> Mn <sub>2.4</sub> Ge <sub>2</sub> (this work)	1.2/2.5	63.1/143
Mn <sub>5</sub> Ge <sub>3</sub> [26]	3.8/9.3	133/440
MnP [27]	3.3/6.0	N/A
MnAs [28]	$30^{a}/32$	$\sim 150^{a}/\sim 576^{a}$
MnFeP <sub>0.45</sub> As <sub>0.55</sub> [29]	14.5/18	174/414
MnCoGe <sub>0.95</sub> Ga <sub>0.05</sub> [30]	14/34	N/A

<sup>&</sup>lt;sup>a</sup> The values were estimated using data from the cited sources.

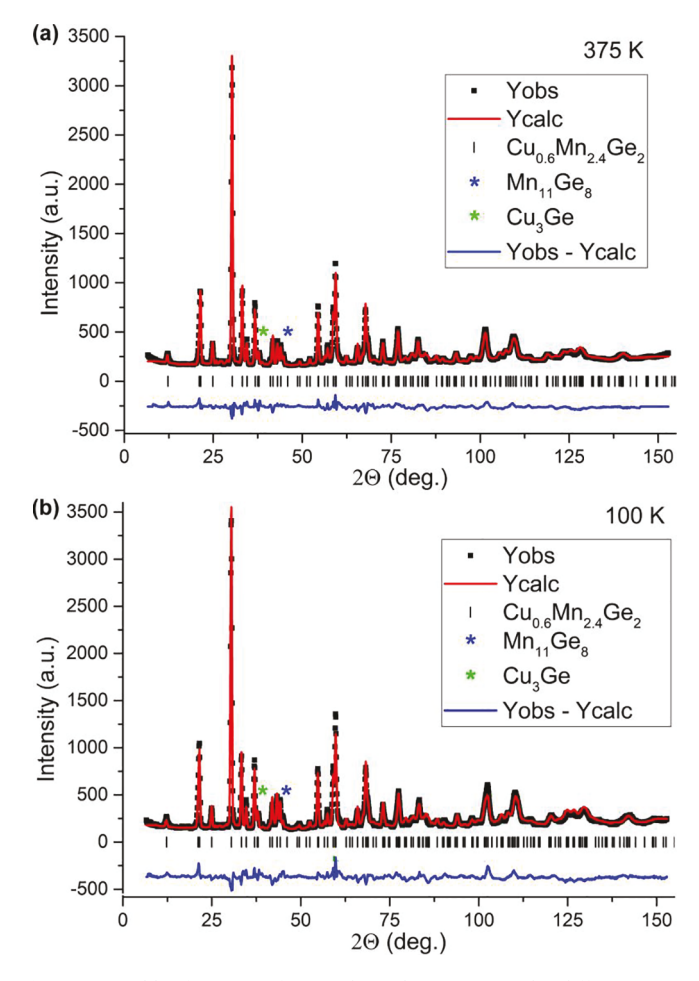


**Fig. 4.** Rietveld refinement of non-polarized neutron powder diffraction patterns of  $\text{Cu}_{0.6}\text{Mn}_{2.4}\text{Ge}_2$  at 375 K (a) and 100 K (b). The simulated profile is shown with a solid red line while the difference between the experimental and simulated data is shown with a solid blue line. The most notable peaks of the impurity phases are indicated with asterisks.

containing materials that exhibit a giant magnetocaloric effect (MCE). Nevertheless, due to the broad —  $\Delta S_{\rm m}$  peak, this material has a relatively high RCP value (Table 1). An interesting possibility exists in this system due to the fact that Cu<sub>0.6</sub>Mn<sub>2.4</sub>Ge<sub>2</sub> possesses hexagonal symmetry (space group  $P6_3/mmc$ ) while the structure of CuFe<sub>2</sub>Ge<sub>2</sub> exhibits an orthorhombic distortion (space group Pmma). Hence, under certain chemical substitution Cu<sub>0.6</sub>Mn<sub>2.4</sub>Ge<sub>2</sub> might show a phase transition between the hexagonal and orthorhombic structures. Indeed, Zavalij *et al.* reported that a related material, Cu<sub>1-x</sub>Co<sub>2+x</sub>Ge<sub>2</sub>, exists in either of these symmetries depending on the Cu/Co ratio defined by the non-stoichiometry index x [10]. If a structural phase transition in Cu<sub>0.6</sub>Mn<sub>2.4</sub>Ge<sub>2</sub> could be triggered by chemical substitution and coupled to the FM ordering, the

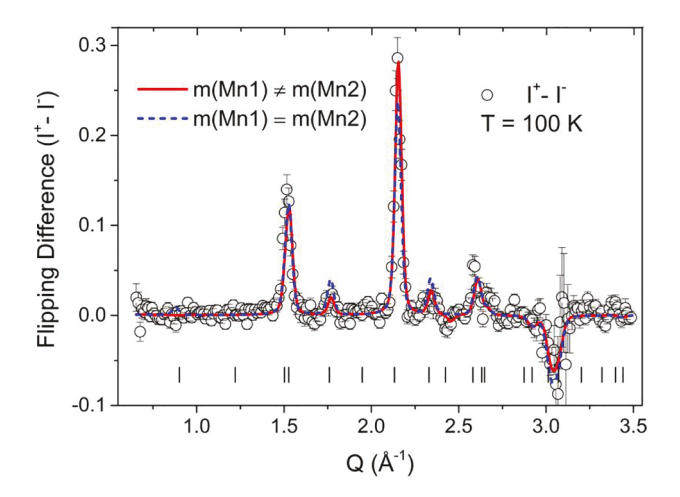


**Fig. 5.** The flipping difference of polarized neutron scattering data obtained on a powder sample of  $Cu_{0.6}Mn_{2.4}Ge_2$  at 100 K. The fit to the data is shown with a solid red line for unrestrained moments in the Mn1 and Mn2 sites and with a dashed blue line for equal moments in these sites. Magnetic peak positions are shown as black lines at the bottom of the figure.

MCE effect might be dramatically enhanced [31].

# 3.3. Neutron diffraction measurements

Non-Polarized Neutron Scattering. To verify the reported nuclear structure of Cu<sub>0.6</sub>Mn<sub>2.4</sub>Ge<sub>2</sub>, a powder sample prepared in the amount of ~ 3 g with the nominal elemental ratio was subjected to non-polarized neutron diffraction at the HB-2A diffractometer. The neutron powder diffraction patterns taken at 375 K and 100 K (Fig. 4) revealed the appearance of magnetic scattering superimposed on nuclear peaks at low scattering angles. The total peak intensity is described by  $I = F_N^2 +$  $F_{M}^{2}$  where  $F_{N}$  and  $F_{M}$  are the nuclear and magnetic structure factors, respectively. This observation is consistent with the ferromagnetic order below  $T_{\rm C}=316$  K, as established by the magnetic measurements. Rietveld refinement performed at 375 K was used to establish non-magnetic contribution to the nuclear peak intensities and refine the content of Cu and Mn in the mixed atomic positions, given the drastically different neutron scattering lengths of these elements (7.718 fm for Cu and -3.73fm for Mn). The refinement also accounted for the minor impurity phases, Mn<sub>11</sub>Ge<sub>8</sub> and Cu<sub>3</sub>Ge.

Representational analysis was carried out using the SARAh software to determine possible models of the magnetic structure. A magnetic phase constructed with Mn moments lying in the *ab* plane provided a good description to changes in intensity observed for the low-angle peaks in the 100 K pattern. A combined refinement of the nuclear and magnetic structures resulted in unequal moments on the Mn1 and Mn2 sites

Polarized Neutron Scattering. In order to verify the unequal moments on the Mn/Cu sites, the same sample was subjected to polarized diffraction measurements using the HYSPEC beamline at ORNL. In contrast to the non-polarized scattering from an FM ordered material, which leads to relatively minor changes in the intensity of nuclear peaks, the polarized scattering allows the enhancement of the FM term by taking the difference between intensities observed for two polarization directions:  $I^{\pm} = F_{\rm N}^2 + F_{\rm M}^2 \pm 2P_0DF_{\rm N}F_{\rm M}$ , where  $P_0$  is the incident neutron beam polarization (86%) and D is the depolarization of the beam passing through the pelletized powder sample [16]. The beam depolarization can result from incomplete saturation of magnetization by the relatively weak field (B=0.4 T) applied in the experiment or from the residual stray magnetic fields due to the permanent magnet yoke hosting the sample. The difference function,  $I^+ - \Gamma = 4P_0DF_{\rm N}F_{\rm M}$ , substantially increases the sensitivity to the magnetic contribution from peaks with

**Table 2** Crystal structure parameters of  $Cu_{0.6}Mn_{2.4}Ge_2$  ( $Cu_{0.6(6)}Mn_{2.27(3)}Ge_2$ ) and the results of Rietveld refinement based on the high-resolution NPD data collected at different temperatures.

Parameter	375 K (NPD, $\lambda = 1.54$ Å)		100 K (N	100 K (NPD, $\lambda = 1.54$ Å)		
a, c (Å) V (Å <sup>3</sup> )	8.1881(3), 5.1684(2) 300.09(2)		8.1445(3), 5.1315(3) 294.79(2) (1.77% change)			
Atomic Site	SOF	<i>x</i> , <i>y</i> , <i>z</i>	SOF	<i>x</i> , <i>y</i> , <i>z</i>		
Cu3 2a	1	0, 0, 0	1	0, 0, 0		
Ge1 2d	1	1/3, 2/3, 1/4	1	1/3, 2/3, 1/4		
Ge2 6 h	1	0.1976(4), 0.3951	1	0.1976(4), 0.3951		
		(4), 3/4		(4), 3/4		
Mn1 6 g	0.69(2)	1/2, 0, 0	0.69(2)	1/2, 0, 0		
Cu1 6 g	0.03(2)	1/2, 0, 0	0.03(2)	1/2, 0, 0		
Mn2 6 h	0.823	0.1573(8), 0.3146	0.823	0.1582(9), 0.3166		
	(2)	(8), 1/4	(2)	(9), 1/4		
Cu2 6 h	0.03(2)	0.1573(8), 0.3146	0.03(2)	0.1582(9), 0.3166		
		(8), 1/4		(9), 1/4		
m(Mn1)	N/A		2.29(9) μ	2.29(9) μ <sub>B</sub> /atom		
m(Mn2)	N/A		$2.7(1) \mu_{B}$	2.7(1) μ <sub>B</sub> /atom		
$R_{\rm p},R_{\rm wp}$	19.7%, 17.6%		23.4%, 2	23.4%, 21.5%		
$R_{\mathrm{Bragg}}$	12.2%		16.2%	16.2%		

 $R_{\rm p}=\Sigma|Y_{\rm o}-Y_{\rm c}|/\Sigma|Y_{\rm o}|;~R_{\rm wp}=\Sigma[w(Y_{\rm o}-Y_{\rm c})^2/\Sigma w(Y_{\rm o})^2]^{V_{\rm s}};~R_{\rm Bragg}=\Sigma|I_{\rm o}-I_{\rm c}|/\Sigma|I_{\rm o}|,$  where  $Y_{\rm o}$  and  $Y_{\rm c}$  are, respectively, observed and calculated profile intensities taken with a 0.05° step and  $I_{\rm o}$  and  $I_{\rm c}$  are the corresponding intensities of Bragg peaks.

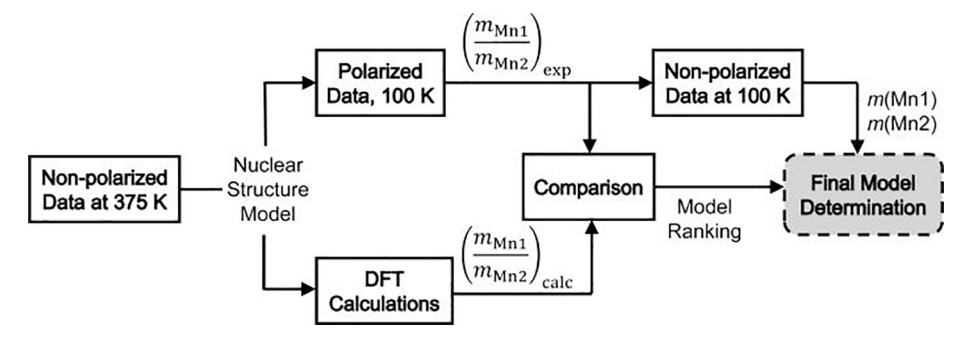
strong nuclear contribution. Assuming the known values of  $F_{\rm N}$ ,  $P_{\rm 0}$ , and D, the FM ordered moments become quantifiable to much higher sensitivity and accuracy. Such quantification, however, is non-trivial for powder samples due to uncertainties in estimating the value of beam depolarization (D), as well as the multitude of structural disorder models that need to be considered in the case of  $\text{Cu}_{0.6}\text{Mn}_{2.4}\text{Ge}_2$ .

To accommodate these challenges, we carried out analyses on all suitable structural models that could fit the data in the paramagnetic state and estimated the depolarization factor from scaling the total Mn magnetization, m(Mn1) + m(Mn2), to the value obtained from the isothermal magnetization measurement (M vs. H). For all tested models, the ratio between the Mn1 and Mn2 moments was found to consistently deviate from unity. Fig. 5 shows the best fit of the flipping ratio profile  $(I^+ - I^-)$  using non-equal Mn1 and Mn2 moments, compared with the fitting result of a constrained equal-moments model. Consequently, the non-polarized data obtained at 100 K, which contain a larger number of Bragg reflections, were used to re-refine the structural parameters and moment amplitudes with the fixed ratio between the Mn1 and Mn2 moments as determined from the polarized data. (Note that the fit of the polarized data suggests the presence of a small induced moment on the Cu3 (2a) site, of the order of <2% of the Mn moment. This moment was ignored in the refinement of the non-polarized data.)

# 3.4. Refinement of crystal and magnetic structures

The crystal structure refinement revealed that the 2a site in the origin of the unit cell was completely occupied by Cu, in agreement with the model proposed by Zavalij  $et\,al.$  [7]. With regard to the occupancy of the transition metal sites  $6\,g$  and  $6\,h$  (Table 2), however, we considered the model used by Zavalij  $et\,al.$  as unlikely. Our electronic structure calculations (see below) showed it would be difficult to justify, based on the difference in total energy, why one site would be completely occupied by Mn atoms while the other site would contain the mixture of Mn, Cu, and vacancies. Therefore, we considered several more realistic disorder models:

- (1) the M1 (6 g) site is partially filled with Mn atoms while the M2 (6 h) site is completely filled with a mixture of Mn and Cu atoms;
- (2) the M2 (6 h) site is partially filled with Mn atoms while the M1 (6 g) site is completely filled with a mixture of Mn and Cu atoms;



Scheme 1. The strategy used in the crystal and magnetic structure determination of Cu<sub>0.6</sub>Mn<sub>2.4</sub>Ge<sub>2</sub>.

Table 3

A comparison of the disorder models based on the ratio of magnetic moments in the Mn1 and Mn2 sites derived from the polarized neutron diffraction data and DFT calculations.

Model	Site	SOF (Mn/Cu)	Mn moment ( $\mu_B$ )	Moment Ratio: m(Mn1)/m(Mn2)		
				polarized neutron data	DFT calculations	difference
1	M1 (6 g)	0.62(2)/0	2.6(1)	1.15	0.72	37%
	M2 (6 $h$ )	0.920(6)/0.080(6)	2.45(9)			
2 M1 (6 g) M2 (6 h)	M1 (6 g)	0.878(7)/0.122(7)	1.81(7)	0.52	1.02	-96%
	M2 (6 h)	0.75(2)/0	3.0(1)			
3a	M1 (6 g)	0.69(2)/0.033	2.29(9)	0.83	0.78	6.0%
M2	M2 (6 h)	0.82(2)/0.033	2.7(1)			
3b	M1 (6 g)	$0.70476(D)^{b}/0.0392(D)^{b}$	2.20(8)	0.79	0.78	1.3%
	M2 (6 h)	$0.81316(D)^{b}/0.02784(D)^{b}$	2.9(1)			
4	M1 (6 g)	$0.76028(D)^{b}/0.04208(D)^{b}$	2.13(8)	0.76	0.79	-3.9%
	M2 (6 h)	$0.83972(D)^{b}/0.02496(D)^{b}$	2.7(1)			

<sup>&</sup>lt;sup>a</sup> The difference was calculated as [1 – ratio(DFT calculations)/ratio(polarized neutron data)].

- (3) both M1 and M2 sites are partially filled with a mixture of Mn and Cu atoms, with the sum of Cu SOFs being fixed to 6.67%; this model also considered that Cu might be distributed equally (Model 3a) or unequally (Model 3b) among sites 6 g and 6 h;
- (4) both M1 and M2 sites are partially filled with a mixture of Mn and Cu atoms, with the sums of Cu SOFs and Mn SOFs fixed to satisfy the stoichiometry  $Cu_{0.6}Mn_{2.4}Ge_2$ .

Note that the full occupancy of both 6 g and 6 h sites would lead to a large deviation from the experimentally determined transition metal to germanium ratio that afforded a nearly phase-pure sample (3.5:2 according to the model vs. 3:2 deduced from the synthetic work and EDS elemental analysis). The results for the crystal structure refinement of Model 3a are summarized in Table 2, while the refinement results for other models, including the calculated values of magnetic moments per Mn atom in each site and the total value of  $M_{\rm sat}$  per f.u., can be found in Table S1. Here we explain how we have arrived at Model 3a as the most reasonable option.

Distinguishing between the structural models with such similar element distributions over the two atomic sites would be very challenging if only the non-polarized neutron diffraction data were used. Therefore, we combined the refinement of the non-polarized data with the results of polarized neutron scattering, magnetic measurements, and DFT calculations. The electronic structure and magnetic moment calculations were performed using the SPR-KKR code that allows the use of partial occupancies in the atomic sites.

Our combined strategy for the crystal and magnetic structure analysis (Scheme 1) was to use the nuclear structure refinement from the non-polarized data at 375 K to inform the models used in the electronic structure calculations and in the treatment of the polarized neutron scattering data. The latter, in turn, allowed a reliable refinement of the ratio of magnetic moments in the Mn1 and Mn2 sites at 100 K. This ratio, m(Mn1)/m(Mn2), was then used as a restraint in the refinement of the

non-polarized neutron diffraction data obtained at 100 K, which allowed the combined refinement of the values of the magnetic moments and atomic parameters on each site. The refined moments on each site were then scaled to be consistent with the experimental magnetic saturation data. Finally, the refined ratio of magnetic moments was compared to the one obtained from electronic structure calculations. The results of these studies are presented in Table 3.

All models described above resulted in comparable values of the residual R-factors and visual quality of fit to the non-polarized neutron diffraction data (Table S1). Nevertheless, it is obvious that Models 1 and 2 lead to a large discrepancy in the ratio of Mn1 and Mn2 magnetic moments determined from the polarized neutron scattering data and DFT calculations. Arguably, such an observation is physically reasonable because it is not clear why Cu atoms, at such small SOF values, would only enter site 6 g but not site 6 h, or vice versa. We found that Models 3a, 3b, and 4 afforded the best agreement between the experimental and calculated ratios of magnetic moments in the Mn1 and Mn2 sites. Models 3b and 4, however, led to unreliable refinement of the SOF values for the Cu and Mn atoms occupying the 6 g and 6 h sites (the strong correlations between variable SOF values of Cu and Mn led to divergent ESDs for these parameters). Thus, we adopted the slightly more constrained Model 3a as the most appropriate converging representation of the crystal structure, despite a slightly larger disagreement between the experimental and calculated m(Mn1)/m(Mn2) ratios as compared to Models 3b and 4.

The strategy described above proved to be very successful in integrating all complementary experimental information with the computation results for a robust analysis of the crystal and magnetic structures. Using the procedure described above and scaling the moments to match the experimental magnetization data led to Model 3a with the magnetic moments  $m(Mn1) = 2.29(9)~\mu_B$  and  $m(Mn2) = 2.7(1)~\mu_B$  at 100 K. When the corresponding SOFs refined for these sites are taken into account, the total magnetization of 3.8(1)  $\mu_B$  determined by the combination of

<sup>&</sup>lt;sup>b</sup> These SOF values could not be refined reliably due to diverging ESDs.

neutron diffraction analysis and DFT calculations is in good agreement with the value  $M_{\rm sat}=3.85~\mu_{\rm B}$  determined by magnetometry.

# 4. Concluding remarks

The powerful combination of polarized and non-polarized neutron scattering, together with the magnetization measurements and electronic structure calculations, has allowed a more reliable determination of the nuclear and magnetic structures of  $\text{Cu}_{0.6}\text{Mn}_{2.4}\text{Ge}_2$ . The resulting composition exhibits the magnetic behavior of a soft ferromagnet, while electronic structure theory validated the crystallographically unique manganese atoms having unequal magnetic moments within the ab plane of the hexagonal crystal structure. The ability to determine the structure–property relationships within a powdered sample material containing not only multiple transition metal elements but also vacant sites suggests that similar experiments and modeling could be extended, with equally consistent results, to hard-to-crystallize transition metal intermetallic compounds.

# **Declaration of Competing Interest**

The authors declare that they have no known competing financial interests or personal relationships that could have appeared to influence the work reported in this paper.

# Acknowledgments

This project was supported by the National Science Foundation (award DMR-1905499). This research used resources at the High Flux Isotope Reactor and Spallation Neutron Source, DOE Office of Science User Facilities operated by the Oak Ridge National Laboratory, and resources at the Advanced Photon Source, a U.S. Department of Energy (DOE) Office of Science User Facility operated for the DOE Office of Science by Argonne National Laboratory under Contract No. DE-AC02-06CH11357. This research also used resources provided by the Materials Characterization Laboratory (FSU075000MAC) at the FSU Department of Chemistry and Biochemistry.

# Appendix A. Supplementary data

Supplementary data to this article can be found online at https://doi.org/10.1016/j.jmmm.2021.167827.

### References

- [1] K.V. Shanavas, D.J. Singh, Plos One 10 (2015), e0121186.
- [2] Y. Zou, Z. Feng, P.W. Logg, J. Chen, G. Lampronti, F.M. Grosche, Phys. Status Solidi RRL 8 (2014) 928–930.
- [3] J. Chen, K. Semeniuk, Z. Feng, P. Reiss, P. Brown, Y. Zou, P.W. Logg, G. I. Lampronti, G.F. Malte, Phys. Rev. Lett. 116 (2016), 127001.
- [4] D.J. Singh, Phys. Rev. B 89 (2014), 024505.
- [5] A.F. May, S. Calder, D.S. Parker, B.C. Sales, M.A. McGuire, Sci. Rep. 6 (2016) 35325.
- [6] K. Aoyagi, N. Uchida, J. Phys. Soc. Jpn. 20 (1965) 617.
- [7] I.Y. Zavalii, V.K. Pecharskii, O.I. Bodak, Izv. Akad. Nauk. SSSR Neorg. Mater. 23 (1987) 1858–1862.
- [8] M. Ellner, J. Less-Common Met. 48 (1976) 21-52.
- [9] F. Laves, H.J. Wallbaum, Z. Angew, Mineral. 4 (1942) 17–46.
- [10] J.Y. Zavalii, V.K. Pecharsky, O.I. Bodak, Kristallografiya 32 (1987) 66-69.
- [11] X'Pert HighScore Plus software v. 2.2b, PANalytical B.V., Almelo, Netherlands, 2006.
- [12] V.O. Garlea, B.C. Chakoumakos, S.A. Moore, G.B. Taylor, T. Chae, R.G. Maples, R. A. Riedel, G.W. Lynn, D.L. Selby, Appl. Phys. A 99 (2010) 531–535.
- [13] J. Rodríguez-Carvajal, Physica B 192 (1993) 55-69.
- [14] A.S. Wills, Physica B 276–278 (2000) 680–681.
- [15] B. Winn, U. Filges, V.O. Garlea, M. Graves-Brook, M. Hagen, C.Y. Jiang, M. Kenzelmann, L. Passell, S.M. Shapiro, X. Tong, I. Zaliznyak, EPJ Web Conf. 83 (2015) 03017.
- [16] E. Lelièvre-Berna, A.S. Wills, E. Bourgeat-Lami, A. Dee, T. Hansen, P.F. Henry, A. Poole, M. Thomas, X. Tonon, J. Torregrossa, K.H. Andersen, F. Bordenave, D. Jullien, P. Mouveau, B. Guerard, G. Manzin, Meas. Sci. Technol. 21 (2010), 055106.
- [17] H. Ebert, D. Ködderitzsch, J. Minár, Rep. Prog. Phys. 74 (2011), 096501.
- [18] M. Ellner, J. Appl. Cryst. 13 (1980) 99-100.
- [19] H. Niida, T. Hori, Y. Yamaguchi, Y. Nakagawa, J. Appl. Phys. 73 (1993) 5692–5694.
- [20] B. Malaman, J. Steinmetz, B. Roques, J. Less-Common Met. 75 (1980) 155-176.
- [21] N. Yamada, K. Maeda, Y. Usami, T. Ohoyama, J. Phys. Soc. Jpn. 55 (1986) 3721–3724.
- [22] G. Kappel, G. Fischer, A. Jaéglé, Phys. Status Solidi A 34 (1976) 691-696.
- [23] O.L. Makarova, A.V. Tsvyashchenko, G. Andre, F. Porcher, L.N. Fomicheva, N. Rey, I. Mirebeau, Phys. Rev. B 85 (2012), 205205.
- [24] Magnetic phase transitions reported for other binary compounds in the Mn-Ge system: TC = 350 K and ~700 K for two FM polymorphs of Mn3.4Ge; TC = 710 K and Tcomp = 400 K for ferrimagnetic Mn5Ge2; TC = 296 K for FM Mn5Ge3; TN = 150 K for AFM Mn2.6Ge.
- [25] V.K. Pecharsky, K.A. Gschneidner, J. Appl. Phys. 86 (1999) 565-575.
- [26] Dagula Songlin, O. Tegus, E. Brück, F.R. de Boer, K.H.J. Buschow, J. Alloys Compd. 337 (2002) 269–271.
- [27] R.A. Booth, S.A. Majetich, J. Appl. Phys. 105 (2009) 07A926.
- [28] H. Wada, Y. Tanabe, Appl. Phys. Lett. 79 (2001) 3302–3304.
- [29] O. Tegus, E. Brueck, K.H.J. Buschow, F.R. de Boer, Nature 415 (2002) 150-152.
- [30] D. Zhang, Z. Nie, Z. Wang, L. Huang, Q. Zhang, Y.-D. Wang, J. Magn. Magn. Mater. 387 (2015) 107–110.
- [31] V. Franco, J.S. Blázquez, B. Ingale, A. Conde, Annu. Rev. Mater. Res. 42 (2012) 305–342.